Materials Horizons

Accepted Manuscript

This article can be cited before page numbers have been issued, to do this please use: D. K. Patel, B. E. Cohen, L. Etgar and S. Magdassi, *Mater. Horiz.*, 2018, DOI: 10.1039/C8MH00296G.

ROYAL SOCIETY OF CHEMISTRY

rsc.li/materials-horizons

View Article Online
DOI: 10.1039/C8MH00296G

Materials Horizons

COMMUNICATION

Fully 2D and 3D printed anisotropic mechanoluminescent objects and their application for energy harvesting in the dark

Received 00th January 20xx,
Accepted 00th January 20xx

DOI: 10.1039/x0xx00000x

www.rsc.org/

Dinesh K. Patel, Bat-El Cohen, Lioz Etgar and Shlomo Magdassi*

We report on new materials' compositions enabling fully printed mechanoluminescent 3D devices by using a one-step direct write 3D printing technology. The ink is composed of PDMS, transition metal ion-doped ZnS particles, and a platinum curing retarder that enables a long open time for the printing process. 3D printed mechanoluminescent multi-material objects with complex structures were fabricated in which light emission results from stretching or wind blowing. The multi-material printing yielded anisotropic light emission upon compression from different directions, enabling its use as directional strain and pressure sensors. The mechanoluminescent light emission peak was tailored to match that of a perovskite material, and therefore, enabled the direct conversion of wind power in the dark into electricity, by linking the printed device to perovskite-based solar cells.

The biggest challenge in 3D printing is to integrate both form and function into the printed object. To overcome this challenge, one needs new functional materials and printing platforms. Among the 3D printing technologies available, direct ink writing (DIW) is a low-cost, high-speed process, based on layer-by-layer dispensing of a viscous liquid, capable of creating complex 3D structures in one step.[1-2] To fabricate structures with good precision and composition, the ink used in DIW should fulfill two criteria: First, the rheological properties of the ink must be tailored so it flows through the dispensing nozzle and facilitates dispensing yet quickly retains the pre-designed shape of the deposited layer(s). Second, it must contain a high proportion of the functional building material, to minimize drying-induced shrinkage after printing.[1] DIW can be utilized for multi-material printing by using several print heads, thus enabling multiple functionalities with forming devices.[3] DIW has been used in myriad applications such as bioelectronics,[3] microfluidics,[4] sensors,[5] wave guides,[6-7] catalyst carriers,[8] data storage,[9] tissue engineering,[10] graphene aerogels,[11] and drug-delivery systems.[12]

Mechanoluminescence was first demonstrated by Francis Bacon in 1605 by breaking sugar crystals.[13-14] During the last few decades, researchers have devoted much attention to developing mechanoluminescent (ML) materials. The main studied ML materials are quartz,[15] rocks,[16] alkali halides,[17-18] molecular crystals,[19] rare earth ion-doped aluminates and silicates[20-21] as well as zinc sulphide (ZnS).[22] Rare earth ion-doped aluminates and silicates, along with ZnS display intense and repeatable mechanoluminescence. ZnS doped with transition metal ions (Cu^{+}, Mn^{2+}, and others) has been well studied for fabrication of ML devices owing to the intense and durable mechanoluminescence.[23-25] Intense, reproducible, and non-destructible ML can be obtained by combing transition metal ion-doped ZnS particles and stress transmission materials.[26] The most common stress transmission materials (transparent elastomeric matrix) are epoxy resin[27] and poly dimethyl siloxane (PDMS).[23, 26] High transparency, low cost, inertness, robustness, and high durability make PDMS an ideal candidate for a stress transmission material for fabricating ML devices with high brightness.[22, 26] Devices comprising PDMS and ZnS were studied for both their fundamental and technological applications,[23] while fabricated by using conventional processes such as casting, molding, and cutting,[23-24, 26] which limit the devices to simple shapes only, by using mainly commercially available materials.[23-26] ML devices have found applications in the fields of flexible sensors,[28-29] dynamic mapping of personal handwriting/signatures,[30] generating light using wind energy,[23] structural health monitoring (SHM) for composite materials/polymers,[31] artificial skin,[32] and piezo-phototronic luminescence devices.[33] 3D printing of ML devices with complex geometries in one step will not only save time and fabrication cost, but would also open a window for a wide variety of new applications based on unique geometries and multi-wavelength emission for directional ML and energy harvesting in dark.

Casali Center for Applied Chemistry, Institute of Chemistry, The Center for Nanoscience and Nanotechnology, The Hebrew University of Jerusalem, Jerusalem 9190401, Israel.
Email: magdassi@mail.huji.ac.il

† Footnotes relating to the title and/or authors should appear here.
Electronic Supplementary Information (ESI) available: [details of any supplementary information available should be included here]. See DOI: 10.1039/x0xx00000x

View Article Online
DOI: 10.1039/C8MH00296G

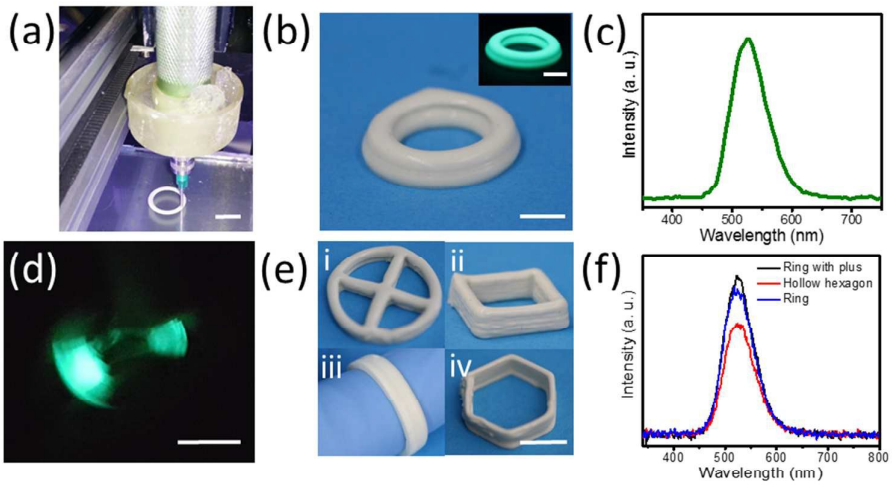

Fig. 1 (a) Printing of a ML device (in process), (b) 3D printed ML candy (inset shows a photograph of green light-emitting candy under UV exposure), (c) a luminescence spectrum generated from the ML candy, (c) a photograph of the ML candy under compression and release, and (e) a ring with plus at the center, a hollow square, ring, hollow hexagon (i-iv), and (f) their ML spectra under continuous stretching and release. The scale bar is 10 mm.

Here, we report for the first time on fully printed 2D and 3D printed ML devices using DIW material printing. The ML devices consist of ZnS doped with transition metal ions, PDMS, and a platinum curing retarder that enables a sufficient open time (Fig. S1a) for performing the printing process. Figure 1a schematically presents the printing process for ML devices. It consists of an extruder loaded with viscous ink; it is externally cooled using an ice and salt mixture. Figure 1b shows a 3D printed ML candy structure, and the inset shows a photo of emitted green light under UV illumination (365 nm). Figure 1c shows the generated ML spectrum and Fig. 1d shows a photo of the object under compression and release (see mechanoluminescence in Movie S1). Figure 1e (i-iv) shows fully printed ML objects having various geometries. These structures show green luminescence under UV exposure at 365 nm (Fig. S2) and green mechanoluminescence upon compression and release (Fig. 1f). The DIW enables even fabrication of 3D printed cube shaped balloons (Fig. S3a), which shows green luminescence upon blowing with compressed air, with a peak centered at 515 nm (Fig. S3b, Movie S2).

The printed objects were tested for their ability to produce light by wind blowing. In the past, wind-driven ML devices were fabricated using multiple steps, i.e., casting on a mold followed by cutting.[23] Similar compositions of inks with various doping of ZnS were printed with the aim of obtaining ML devices for light harvesting. Figure 2a demonstrates fully printed wind-driven ML objects having different light emission

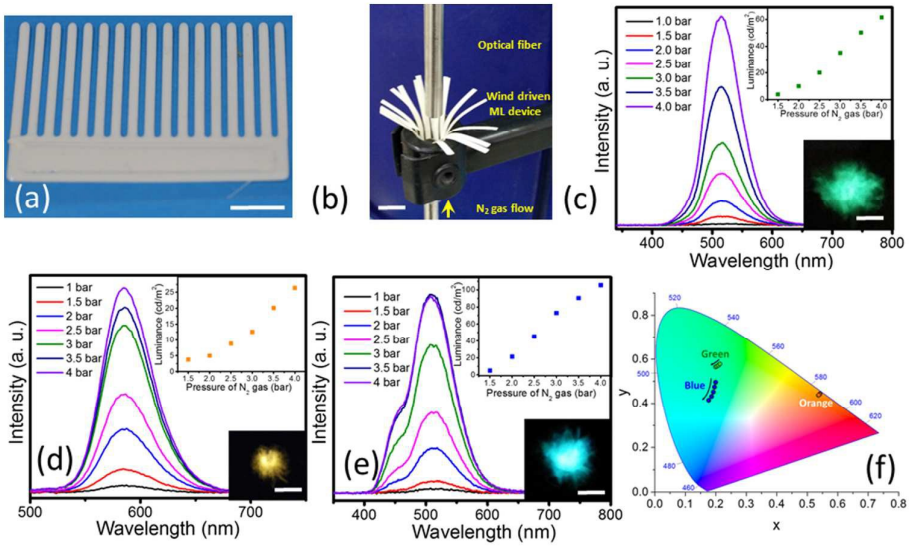

Fig. 2 (a) A fully printed wind-driven ML device; (b) a setup for measuring ML from a printed wind-driven device; (c-e) ML spectra of wind-driven green (c), orange (d), and blue (e) devices (upper insets show the luminance with varying pressures of nitrogen gas flow, and the lower insets show photographs of corresponding ML devices and (f) CIE from wind-driven green, orange, and blue ML devices. The scale bar is 10 mm.

View Article Online
DOI: 10.1039/C8MH00296G

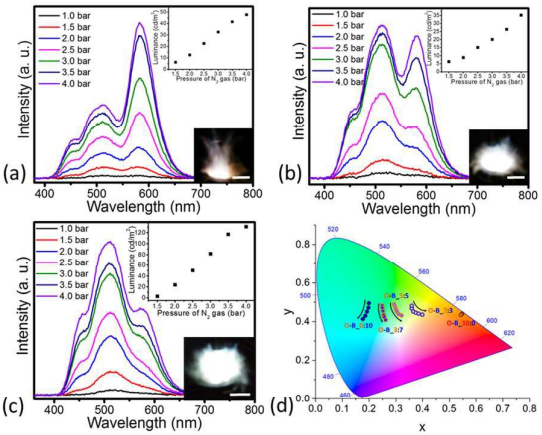

Fig. 3 Fully printed wind-driven ML devices with different ratios of orange- and blue-emitting ZnS in PDMS matrix; ratio: (a) 7:3, (b) 5:5, and (c) 3:7 (insets show the luminance under varying pressures of nitrogen gas flow and the lower insets show photographs of luminescence from the devices), (d) CIE from wind-driven ML for different ratios of orange (O) to blue (B) from 0:10 to 10:0. The scale bar is 10 mm.

spectra. The thickness of these wind driven ML devices were about 700-800µ. The setup used to generate light by wind (here by nitrogen gas, whereas the flow rate is controlled by the gas cylinder pressure) is shown in Fig. 2b. The dependence of ML intensity and spectra on gas flow for various doping of the ZnS particles is shown in Fig. 2c,d,e (green, orange, and blue) and Movie S3. As presented, for all objects, increasing the flow rate led to an increase in the emitted light intensity, whereas the positions of the emission peaks were almost unchanged (515 and 586 nm, respectively), except for the blue-emitting object for which we observed a blue shift (Fig. S4). Figure 2d shows the CIE plot of the emitted light. For a blue wind-driven ML device, a significant shift in CIE coordinates (0.20, 0.53 to 0.18, 0.42) was observed, but for a green-emitting ML device, a minimal shift was observed. For an orange wind-driven ML device, there was no shift in the CIE coordinates (Fig. 2f).[23-24]

With knowledge of the CIE plots, we aimed at preparing white ML light by combining orange- and blue-emitting phosphors. Figure 3 (a-c) shows the emission spectra obtained from printed wind-driven ML objects containing different weight ratios of orange and blue phosphor, i.e., 7:3, 5:5, and 3:7. The upper inset shows the dependence of luminance intensity on the gas flow rate and the lower inset shows a photo from the wind-driven objects. Luminance observed in our study from orange and blue phosphor with a 3:7 ratio was around 132 cd/m^2 (Movie S4), which is much higher than previous reports on ML for generating white light (50 cd/m^2 and 21 cd/m^2).[23, 33] Jeong et al have used orange and blue phosphor in ratio 7:3[23] whereas Chen et al have used a commercial white phosphor with unknown composition for generation of white light.[33] Figure 3d shows the CIE diagrams of these devices with different weight ratios of orange and blue-emitting ZnS. It was observed that an increase in the weight ratio of blue phosphor results in a systematic shift from orange towards white light. These results are in agreement with previous reports.[23] As seen in Fig. S5, we could generate cool white light using a weight ratio of orange:blue ZnS (7:3) with a correlated color temperature (CCT) of 3861 K; the CIE coordinates lie on black body radiation (Planckian locus). Wind driven ML devices have been demonstrated earlier for light harvesting including white light generation, but were fabricated with conventional and time consuming processes,

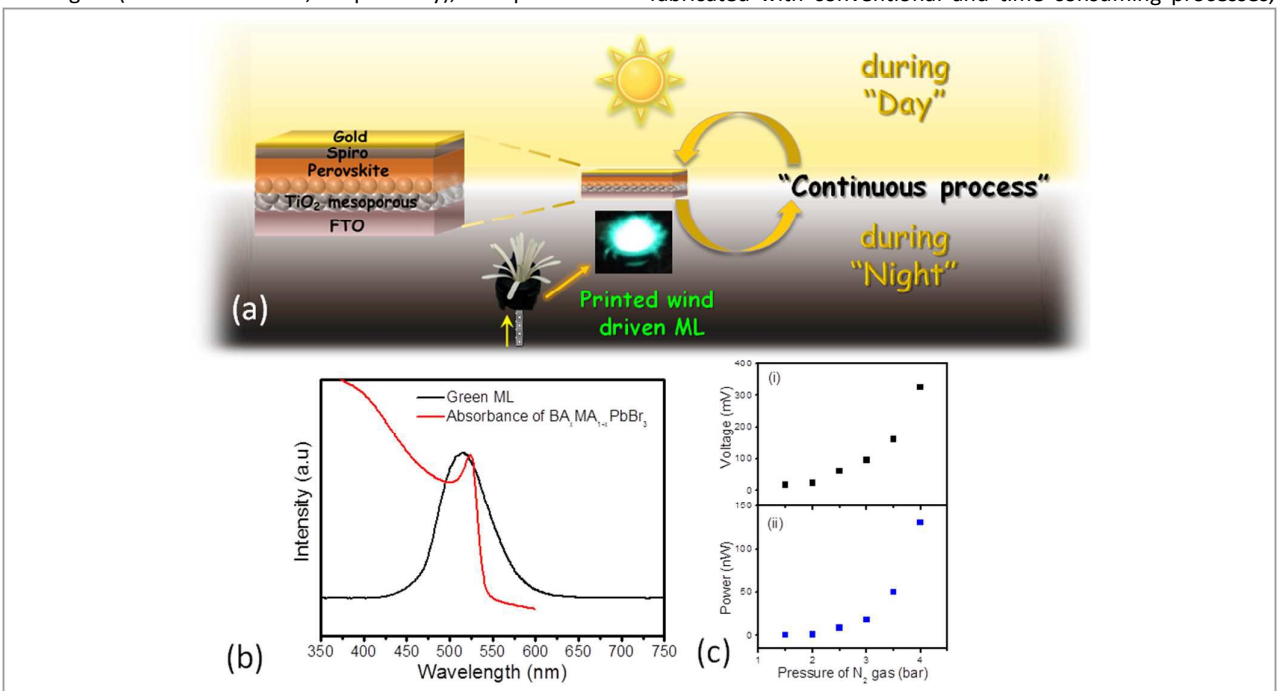

Fig. 4 (a) Schematic representation of energy harvesting in the dark using a wind-driven ML device and a perovskite-based solar cell, (b) Absorbance for a perovskite-based solar cell and ML emission from a wind-driven ML device with green phosphor, (c) voltage and power generated by a wind-driven ML device coupled with a perovskite-based solar cell.

View Article Online
DOI: 10.1039/C8MH00296G

moulding and cutting.[23,26] By the proposed process we overcome these drawbacks and provide a simple additive manufacturing process with tailored materials composition.

Such printed wind-driven ML devices were further evaluated for energy harvesting. Solar energy harvesting can be performed only at daytime by using solar cells or thermosolar devices. If the solar cells can also function at night, this will be a significant advantage. We suggest performing energy harvesting using solar cells in the dark, while the solar cell is illuminated with light generated by wind-driven ML devices. The schematic representation of energy harvesting in the dark using a perovskite solar cell linked to a wind-driven ML device is shown in Fig. 4a. The main requirement for this approach is to match the ML spectra to the absorption spectra of the perovskite. Indeed, the absorbance of the perovskite layer is shown in Fig. 4b; the layer has a strong absorbance (n= ∞) around 520 nm, whereas the green wind-driven ML device displays emission maxima of around 515 nm. Thus, absorbance from the perovskite and green ML emission overlap well; hence, it can be used for energy harvesting. In this setup, the solar cell was placed above the wind-driven ML devices and it was illuminated by light obtained from ML generated by nitrogen flow, at varying pressures. The output voltages and power generated are shown in Fig. 4c. It was observed that, with an increase in the pressure of nitrogen gas, the voltage and power generated increases. We also carried out the same experiment with a wind-driven ML device with orange and blue phosphor in a 5:5 ratio for energy harvesting in the dark (Fig. S6). We observed that the voltage and current generated from this device is lower compared with the green-emitting device (Fig. S6b) since luminance (Fig. 3b, upper inset) is lower compared with that of the green ML devices (Fig. 2c, upper inset). Terasaki et al have demonstrated energy harvesting from ML device using $SrAl_2O_4$:Eu pellet and single crystal silicon based solar cell. ML was generated by applying different loads on $SrAl_2O_4$:Eu pellet and the process was destructive.[34] In our report, we used wind driven ML for energy harvesting in dark, by combing a printed ML object with a perovskite based solar cell and its absorption can be tuned. The power generated in this process is higher than previously reported, but at this point it is lower than that obtained during the day time. Therefore future efforts will be directed towards increasing the light emission output.

Utilizing 3D printing technologies enables the structuring of ML objects composed of multimaterials that are localized in functional shapes. Figure S7 a, d presents, fully printed

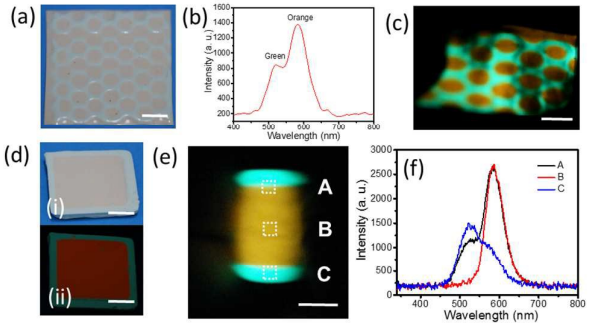

Fig. 5 Dual light-emitting patterned ML devices: (a) photo of patterned hexagonal mesh, (b) ML from hexagonal mesh emitting green and orange, (c) a photograph of the hexagonal mesh under stretching and release, (d) a concentric square (i) without and (ii) under UV illumination (365 nm), (e) a ML image and (f) a ML spectrum at three regions: A, B, and C. The scale bar is 10 mm.

patterned green/orange ML square and hexagonal meshes (thickness around 1 mm) that emit light upon stretching (Fig. S7c, Movie S5), which were printed within 10 minutes. For a comparison, Jeong et al. have demonstrated the fabrication of multicolor-patterned devices using a complex multiple step process; the time required to fabricate the device was around 5 days.[35] This device could emit a light pattern only if both an electric field and stretching are applied.[35]

DIW technology enables printing objects composed of multi-materials in a simple one-step process, as presented in Fig. 5 for a hexagonal ML mesh having dual emission capability. The ML spectra generated from these mesh (by stretching and release), along with a photo showing green and orange light, is shown in Fig. 5 b and c (video S6). We also printed concentric squares with an inner region that emits orange and an outer region that emits green (Fig. 5d). The thickness of this device was 3 mm. Figure 5d (ii) shows the patterned image under excitation at 365 nm and Fig. 5e shows a photo of a concentric square during compression and release. Figure 5f shows an ML spectrum of a fully printed concentric square upon compression and release. ML spectra were recorded at three different regions (A, B, and C) as seen in Fig 5e. 'A' corresponds to the interface between the two regions, yielding both green and orange emission (the intensity of orange emission at 586 nm is higher than that at 515 nm), 'B' corresponds to the center region and has only orange emission (586 nm), and 'C' corresponds to the outer region

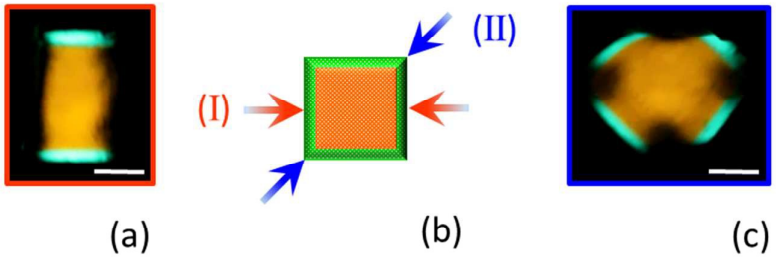

Fig. 6 Anisotropic mechanoluminescent (AML) device: photograph of an AML device on (a) horizontal compression and release from the sides (I, shown by red arrows), (b) schematic representation of an AML device, and (c) diagonal compression and release (II shown by blue arrows). The scale bar is 10 mm.

View Article Online
DOI: 10.1039/C8MH00296G

having mainly green emission (Fig. 5f). It should be emphasized that the objects with dual ML emission are fabricated in one printing process, without assembling parts, which is required by a conventional fabrication process. Furthermore, the dual emission enables a directional/anisotropic response, as shown in Fig 6. We fabricated an 'anisotropic' mechanoluminescent (AML) device showing different ML light patterns while compressed in different directions. When the AML device is compressed and released from the sides, i.e., horizontally, we observed two green lines on the opposite sides and orange light at the center. Similarly, when an AML device is compressed from the opposite corners, i.e., diagonally, we observed four green patterns on all sides (except the corners) and orange light at the center (Movie S7). Clough et al. reported tensile anisotropy using mechanoluminescent dioxetane and elastomer, but the emission was not visible to the naked eye, and different magnitudes of strain must be applied to obtain the signal, which is recorded by a sophisticated instrument/camera.[36]

Conclusions

In summary, we reported fully printed ML devices of various geometries using the DIW technique. Wind-driven ML devices were printed in one step for the first time, and cool white light having a CCT of 3861 K and 48 cd/m^2 luminance was obtained from objects consisting of orange and blue phosphor. In this report, we have demonstrated a proof of concept for a small device for direct conversion of wind power to electricity by linking them to perovskite-based solar cells. At present the power generated is low and efforts are needed to improve the performance in large scale operation. This can be achieved by increasing the ML intensity through the use of multiple ML devices in parallel, or search for materials which have higher ML intensity. Future efforts will be directed in this direction. We also demonstrated patterned ML devices that can emit single or dual colors. An anisotropic light ML emission was obtained upon compression from different directions, enabling its use as directional strain sensors. We expect that these findings will lead to new mechanoluminescence-based applications such as embedded sensors, security inks, and energy devices.

Experimental

Ink formulation for printing ML structures: To fabricate the colored 2D and 3D printed ML structures, ML phosphor materials were mixed in PDMS. PDMS base (Elastosil RT 601 A, Wacker) and cross-linker (Elastosil RT 601 B, Wacker) were weighed in a 9:1 ratio along with 1% by weight of platinum silicone cure retarder (SLO-JO, Smooth-On, Inc.) with respect to PDMS, which were mixed in a Thinky mixer for 2 min. The required amounts of ML material (Green GGS 42, Orange GG13, and Blue GGS 62, Mobichem Scientific Engineering, Ltd.) were added to PDMS and stirred manually with the help of a glass rod. The ML material:PDMS weight ratio was maintained at 7:3. Mechanical properties of these compositions were evaluated and discussed in Fig. S1.

3D printing: ML devices were printed using System 30M (Hyrel 3D, USA), using a metallic extruder coupled with a nozzle with a size of 1.02 mm (18G). The thickness of each printed layer is around 500 µ. The build platform temperature was maintained at 40-50 °C. All ML structures were printed with a PDMS:phosphor ratio of 3:7 along with 1% curing retarder. The extruder was externally cooled by an ice-salt mixture, presented in Fig. 1a to further increase the open time of the ink. The use of the curing retarder and the external cooling (T= 0-5 °C) enabled an open time for a printing time of at least 30 minutes. The extrusion of the ink was controlled using Gcode with REPETREL software provided by Hyrel Systems.

Perovskite cell fabrication: Perovskite precursor synthesis: Methyl ammonium bromide (MABr) and benzylammonium bromide (BABr) were synthesized for fabrication of cells, as reported earlier and were used as precursors for fabrication of perovskite-based cells.[37]

Cell fabrication: SnO_2:F (FTO) conductive glass (15 Ωcm^{-1}, Pilkington) substrate was coated by a TiO_2 compact layer (5000 rpm 30 sec) prepared from a precursor solution of titanium diisopropoxide bis(acetylacetonate) (Sigma) in anhydrous ethanol (0.2:1 (v:v)) and was annealed at 450 °C, 30 min. TiO_2 nanoparticle paste (20 nm, dyesol) was diluted to a 1:4 ratio in ethanol absolute (Sigma) and spin-coated (5000 rpm, 30 sec) onto this substrate and annealed at 500 °C, 30 min. The substrate was then treated with $TiCl_4$ (70 °C, 30 min) and annealed again at 450 °C for 30 min. The perovskite layer was deposited on the substrate by two-step spin coating (10 sec 1000 rpm + 60sec 5000 rpm) from a precursor solution containing BABr (0.08 mM), MABr (2M), and $PbBr_2$ (2.05 M) in γ-butyrolactone / dimethylsulphoxide (1:1 (v:v)). During the second spin coating, 40 µL of toluene were added dropwise on the perovskite layer. After the perovskite was deposited, the films were annealed at 110 °C for 1 hour. The hole transporting layer was deposited onto the substrates by spin coating of a 40µL solution at 4000 rpm for 30 sec after an initial 30 sec of loading time. The HTM solution contains 0.072 g 2,2',7,7'-tetrakis-(N,N-di-4-methoxyphenylamino)-9,9'-spirofluorinein, 1ml chlorobenzene with additives of 17.5 µL/1ml bis(trifluoromethane)sulfonimide lithium salt in acetonitrile (520 mg/ml), and 28.8 µL/1ml of 4- tert –butilpyridine (Aldrich). A ~70 nm-thick gold electrode was thermally evaporated on the film under a vacuum of ~10^{-7} Torr. Perovskite and hole transporting layer depositions took place in a nitrogen-filled glove box.

Energy harvesting in the dark: A perovskite cell was connected to a voltage/current-measuring device and was placed above a wind-driven ML device, as seen in Fig. 4a. The varying pressure of N_2 gas was passed through a wind-driven ML device and the

View Article Online
DOI: 10.1039/C8MH00296G

output was measured using a voltmeter (EX310 multi-meter, Extech instruments) and a Keithley 2400 source meter (a Tektronix company).

Characterization: ML spectra were monitored through a fiber-coupled StellarNet BLUE-Wave spectrometer. All ML spectra were recorded with a 2s integration time and 0.5 nm resolution in the range of 340 to 1100 nm at room temperature. The CIE coordinates and CCT were calculated from the ML spectra. Illuminance was measured using a Digital Lux Meter, Dr. Meter, LX1330B, China, and was converted into brightness/luminance as reported.[38] The photos and videos were recorded using a Canon EOS 1200D camera equipped with Tamron SP Di macrolens. The rheologies of the inks were measured using Rheo Stress 6000 Rheometer (Thermo Scientific) and mechanical properties of the resins (Fig. S1) were evaluated using Universal Testing Machine (INSTRON 3345, 500 N load cell) as reported earlier.[39]

Conflicts of interest

There are no conflicts to declare.

Acknowledgements

This research was partially supported by the Singapore National Research Foundation, Prime Minister's Office, Singapore under the CREATE program: Nanomaterials for Energy and Water Management, and by the Israel National Nanotechnology Initiative FTA project on functional coatings and printing.

References

1 J. A. Lewis, *Adv. Funct. Mater.*, 2006, **16**, 2193-2204.
2 J. A. Lewis, J. E. Smay, J. Stuecker and J. Cesarano, *J. Am. Ceram. Soc.*, 2006, **89**, 3599-3609.
3 A. E. Jakus, E. B. Secor, A. L. Rutz, S. W. Jordan, M. C. Hersam and R. N. Shah, *ACS Nano*, 2015, **9**, 4636.
4 J. Moorthy, G. A. Mensing, D. Kim, S. Mohanty, D. T. Eddington, W. H. Tepp, E. A. Johnson and D. J. Beebe, *Electrophoresis*, 2004, **25**, 1705-1713.
5 J. H. Holtz and S. A. Asher, *Nature*, 1997, **389**, 829-832.
6 D. N. Christodoulides, F. Lederer and Y. Silberberg, *Nature*, 2003, **424**, 817-823.
7 S. T. Parker, P. Domachuk, J. Amsden, J. Bressner, J. A. Lewis, D. L. Kaplan and F. G. Omenetto, *Adv. Mater.*, 2009, **21**, 2411-2415.
8 G. S. Chai, I. S. Shin and J. S. Yu, *Adv. Mater.*, 2004, **16**, 2057-2061.
9 D. A. Parthenopoulo and P. M. Rentzepis, *Science*, 1989, **245**, 843-845.
10 J. Y. Kim and D.-W. Cho, *Microelectron. Eng.*, 2009, **86**, 1447-1450.
11 C. Zhu, T. Y.-J. Han, E. B. Duoss, A. M. Golobic, J. D. Kuntz, C. M. Spadaccini and M. A. Worsley, *Nat. Commun.*, 2015, **6**, 6962.
12 Y. Y. Li, F. Cunin, J. R. Link, T. Gao, R. E. Betts, S. H. Reiver, V. Chin, S. N. Bhatia and M. J. Sailor, *Science*, 2003, **299**, 2045-2047.
13 F. Bacon, New York, PF Collier & Son **1902**, 45.
14 F. Bacon, *Advancement of learning and Novum Organum*, Vol. 18, Colonial Press, **1900**.
15 G. N. Chapman and A. J. Walton, *J. Appl. Phys.*, 1983, **54**, 5961-5965.
16 Y. Enomoto and H. Hashimoto, *Nature*, 1990, **346**, 641-643.
17 A. J. Walton, *Adv. Phys.*, 1977, **26**, 887-948.
18 B. P. Chandra, A. K. Bagri and V. K. Chandra, *J. Lumin.*, 2010, **130**, 309-314.
19 B. P. Chandra and J. I. Zink, *J. Chem. Phys.*, 1980, **73**, 5933-5941.
20 M. Akiyama, C.-N. Xu, Y. Liu, K. Nonaka and T. Watanabe, *J. Lumin.*, 2002, **97**, 13-18.
21 N. Terasaki, H. Zhang, H. Yamada and C.-N. Xu, *Chem. Commun.*, 2011, **47**, 8034-8036.
22 V. K. Chandra, B. P. Chandra and P. Jha, *Appl. Phys. Lett.*, 2013, **103**, 161113.
23 S. M. Jeong, S. Song, K.-I. Joo, J. Kim, S.-H. Hwang, J. Jeong and H. Kim, *Energy Environ. Sci.*, 2014, **7**, 3338-3346.
24 S. M. Jeong, S. Song and H. Kim, *Nano Energy*, 2016, **21**, 154-161.
25 S. W. Shin, J. P. Oh, C. W. Hong, E. M. Kim, J. J. Woo, G.-S. Heo and J. H. Kim, *ACS Appl. Mater. Interfaces*, 2016, **8**, 1098-1103.
26 (a) S. M. Jeong, S. Song, S.-K. Lee and B. Choi, *Appl. Phys. Lett.*, 2013, **102**, 051110; (b) S. M. Jeong, S. Song, S.-K. Lee and N. Y. Ha, *Adv. Mater.*, 2016, **25**, 6194–6200.
27 X. Chao-Nan, Z. Xu-Guang, A. Morito, N. Kazuhiro and W. Tadahiko, *Appl. Phys. Lett.*, 2000, **76**, 179-181.
28 N. Terasaki and C. N. Xu, *IEEE Sens. J.*, 2013, **13**, 3999-4004.
29 Y. Gun Jin, R. Mohammad Reza, G. Amir Hossein, L. Gong-Cheol and C. Jun-Seong, *Smart Mater. Struct.*, 2013, **22**, 055006.
30 X. Wang, H. Zhang, R. Yu, L. Dong, D. Peng, A. Zhang, Y. Zhang, H. Liu, C. Pan and Z. L. Wang, *Adv. Mater.*, 2015, **27**, 2324-2331.
31 K. Srivatsava, W. Hugo Van der, V. Vijay and S. Vishnu Baba, *J. Intell. Mater. Syst. Struct.*, 2017, **28**, 2458-2464.
32 C. N. Xu, T. Watanabe, M. Akiyama and X. G. Zheng, *Appl. Phys. Lett.*, 1999, **74**, 1236-1238.
33 L. Chen, M.-C. Wong, G. Bai, W. Jie and J. Hao, *Nano Energy*, 2015, **14**, 372-381.
34 N. Terasaki, C.-N. Xu, Y. Imai and H. Yaamada, *Jpn. J. Appl. Phys.*, 2007, **46**, 2385-2388.
35 S. M. Jeong, S. Song, H. Kim, K.-I. Joo and H. Takezoe, *Adv. Funct. Mater.*, 2016, **26**, 4848-4858.
36 J. M. Clough, C. Creton, S. L. Craig and R. P. Sijbesma, *Adv. Funct. Mater.*, 2016, **26**, 9063-9074.
37 B.-E. Cohen, M. Wierzbowska and L. Etgar, *Sustainable Energy Fuels*, 2017, **1**, 1935-1943.
38 E. F. Schubert, *Light-Emitting Diodes*, Cambridge Univ. Press, Cambridge, UK **2006**.
39 D. K. Patel, A. H. Sakhaei, M. Layani, B. Zhang, Q. Ge and S. Magdassi, *Adv. Mater.*, 2017, **29**, 1606000.

View Article Online
DOI: 10.1039/C8MH00296G

Conceptual insights' statement

Mechanoluminescent (ML) materials have been reported for applications such as flexible sensors, dynamic mapping of personal signatures and generating light using wind energy. These devices were fabricated by using conventional processes such as casting, molding, and cutting, which limit the devices to simple shapes only, mainly utilization of one light emitting material, and the fabrication process is time consuming. We present a new process and materials compositions to fabricate devices with complex structures and multimaterial. The process is based on 3D printing of ML materials embedded within elastomeric monomers, by using a direct ink write (DIW) technology. The printing composition contained a curing retardant agent that enabled a long open time of the ink, thus overcoming pre-mature curing and blockage of the printing nozzle. Multimaterial printing enabled patterning ML objects with multiple color emission that can be used in generating anisotropic light emission which acts as a directional sensor. In addition, we printed wind-driven ML devices, in one step, and coupling them with solar cells led to direct converting wind energy into electricity in the dark. By using perovskite based solar cells, tailoring the absorbing material in the cell to the specific light emission of the ML device, enabled power generation higher than reported previously. We expect that these findings will lead to new ML-based applications such as embedded directional sensors, security inks and energy devices.

View Article Online
DOI: 10.1039/C8MH00296G

Fully 2D and 3D printed anisotropic mechanoluminescent objects and their application for energy harvesting in the dark

Dinesh K. Patel, Bat-El Cohen, Lioz Etgar and Shlomo Magdassi*

Casali Center for Applied Chemistry, Institute of Chemistry, The Center for Nanoscience and Nanotechnology, The Hebrew University of Jerusalem, Jerusalem 9190401, Israel
E-mail: magdassi@mail.huji.ac.il

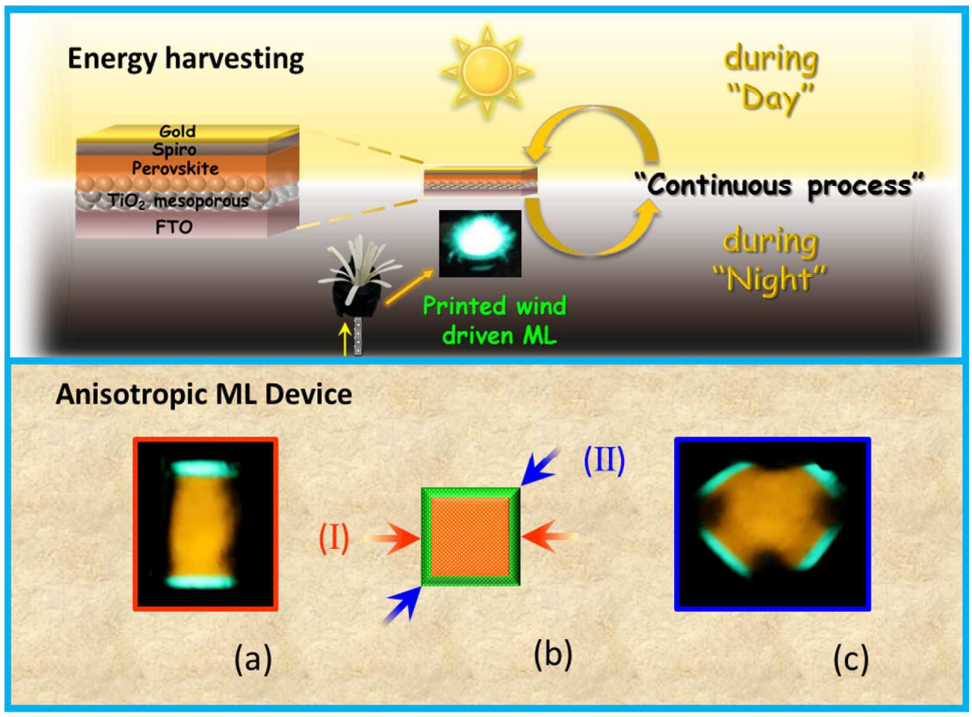

Keyword: 3D printing, PDMS, ZnS, mechanoluminescence, DIW, multi-material printing.